# PHEDRE—Numerical Model for Combustion Stability Studies Applied to the Ariane Viking Engine

M. Habiballah,* D. Lourme,† and F. Pit‡
*Office National d'Etudes et de Recherches Aérospatiales, Châtillon, France*

**A comprehensive numerical model for a direct simulation of high-frequency instabilities is presented. It consists of solving the balance equations of the gaseous phase and the discrete phase (droplets) for given droplet atomization and droplet vaporization data. The model was used for the Ariane Viking liquid propellant engine behavior study in both steady and unsteady configurations. A stability criterion based on the pressure excitation has been found to fit the main features of the actual behavior of the engine.**

## Nomenclature

| | |
|---|---|
| $b$ | = width of the chamber |
| $c_p$ | = specific heat at constant pressure |
| $cv_m$ | = volume fraction of droplets belonging to group $m$ ($\equiv \rho_m/\rho_L$) |
| $e$ | = specific internal energy of mixture |
| $e_k$ | = specific internal energy of species $k$ |
| $i$ | = cell index in the $z$ direction |
| $j$ | = cell index in the $y$ direction |
| $M_k$ | = molar mass of species $k$ |
| $n_m$ | = number of droplets per unit volume belonging to group $m$ |
| $p$ | = pressure |
| $P_s$ | = steady-state mean pressure |
| $R$ | = gas constant or the chamber radius |
| $t$ | = time |
| $T$ | = temperature |
| $u,v$ | = gas velocities in the $z$ and the $y$ directions, respectively |
| $u_m,v_m$ | = droplet velocities in the $z$ and the $y$ directions, respectively |
| $\dot{w}$ | = total mass-source term |
| $\dot{w}_k$ | = mass source, Eq. (2) |
| $\dot{w}_m$ | = mass source, Eq. (6) |
| $y = R\theta$ | = transverse direction |
| $z$ | = axial direction |
| $\mu_g$ | = gaseous phase laminar viscosity |
| $\rho$ | = total density |
| $\rho_L$ | = liquid-jet density |
| $\rho_k$ | = partial density of species $k$ |

*Subscripts*

| | |
|---|---|
| $k$ | = species $k$ |
| $m$ | = group $m$ |
| $ri$ | = radial injection |
| 1 | = gaseous unisymmetrical dimethyl hydrazine (UDMH) |
| 2 | = gaseous $N_2O_4$ |
| 3 | = burned products |

## I. Introduction

HIGH-FREQUENCY instabilities consisting of the combustion excitation of the chamber acoustic modes can be very severe for liquid-propellant rocket engines. In the past, the problem was mainly solved by experimental means, and most of the theoretical work (due to limited computation capabilities) was restricted to linear analyses.

After the Ariane second flight failure resulting from such instabilities in the first-stage Viking engine, and simultaneous with the empirical solutions of the immediate problem,[1] a comprehensive study was started at Office National d'Etudes et de Recherches Aérospatiales (ONERA) to improve the understanding of the phenomenon with a view to the future of Ariane. The Viking engine uses $N_2O_4$ and unisymmetrical dimethyl hydrazine (UDMH), radially injected into the combustion chamber through like-on-like doublets. In practice, three topics have been investigated in parallel: atomization-combustion-aerothermodynamics. The atomization study had to provide the aerothermodynamics with the droplet size and velocity distributions near the injector,[2] and the combustion study had to supply it with the unsteady vaporization-combustion laws of these droplets taking into account the relative gas-droplet velocity.[3] This paper will focus on the aerothermodynamics whose objective was to develop a chamber model for numerical simulation.

## II. Methodology

The objective of the final model was to describe the reactive, unsteady, turbulent, two-phase flow in a combustion chamber with radial injection for given atomization and droplet-combustion data. In fact, three numerical models have been developed: a two-dimensional $(x,y)$ Lagrangian model (Lagrangian equations for the droplets), a two-dimensional $(x, y)$ Eulerian model (Eulerian equations for the droplets), and an annular Eulerian model called PHEDRE. The first two models were developed to gain experience in numerical modeling before beginning the development of the final numerical model; these models had to be validated by specific tests. The final model for the unsteady behavior simulation is the annular one. It uses the same numerical method and the same physical modeling as the planar two-dimensional Eulerian model. For the most part, this article focuses on describing the annular model and also on presenting the results obtained with this model. Results obtained with the two-dimensional $(x,y)$ Lagrangian and the two-dimensional $(x,y)$ Eulerian models will be summarized.

## III. Planar Two-Dimensional Models

### A. Planar Two-Dimensional Lagrangian Model

This model consists of a numerical code which solves 1) the Navier-Stokes equations for the gaseous phase and 2) a set of ordinary differential equations for droplets (Lagrangian equations). The turbulence is described by the classical $k$-$\varepsilon$ turbulence model.

Received Oct. 19, 1988; revision received Aug. 10, 1989. 

*Adjoint Division Chief, Liquid Propellant Engines and Launchers.
†Coordinator for Space Activities.
‡Research Engineer.

This numerical model is well adapted for describing in detail interactions between droplets and gas. One of its objectives was to help validate assumptions (turbulence modeling, for example) made on the annular model. As an experimental support to this code, a two-dimensional transparent chamber was manufactured. Test firings were performed, and experimental data were obtained. Figure 1 gives a comparison of computed droplet velocities with those obtained from streak photography experiments. Agreement is good for the mean velocity $\bar{V}$, although the standard deviation $\sigma$ is not as well predicted.

### B. Planar Two-Dimensional Eulerian Model

The planar two-dimensional Eulerian model was the first step in the annular model development. Its objective was to adjust the numerical approach that would be selected for the annular model. This numerical approach is largely discussed in the following sections. Results obtained with the planar two-dimensional Eulerian model were not directly compared to test results but rather to results obtained with the Lagrangian model. Figure 2 shows a comparison of steady-state results between the two numerical models. The figure concerns the gaseous UDMH mass fraction, pressure, and temperature contours. Agreement is satisfactory and makes it possible to think that the main physical phenomena are quite well described in the Eulerian model.

## IV. Annular Model—PHEDRE

The main purpose of these stability studies was to develop a numerical code for simulating the unsteady behavior of the Viking engine combustion chamber. The Viking engine combustion chamber is axisymmetrical (Fig. 3). Propellants are injected radially. Different acoustic modes may be excited when instabilities occur: radial modes, tangential modes, or combined modes. The most critical, however, are the tangential modes, which often lead to destruction of the engine. The logical approach consists of developing a three-dimensional $(r,\theta,z)$ model. Another alternative was initially chosen: a numerical code was developed, which could simulate tangential modes in a computational annular chamber; the latter is equivalent to the real chamber—this is the PHEDRE code. The numerical approach used in PHEDRE and the results obtained are discussed below.

### A. Governing Equations

The two-phase reactive flow in the combustion chamber of a liquid propellant rocket engine involves various complex phenomena: turbulent mixing and diffusion, droplet heat-up and evaporation, species diffusion, chemical reaction, etc. The gaseous phase consists of a reactive species mixture, and the liquid phase consists of droplets having different diameters, velocities, and temperatures. The two phases exchange mass, momentum, and energy.

In this model, the gaseous phase is assumed to be composed of three main species: fuel (UDMH), oxidizer ($N_2O_4$) and burned products ($P$). Note that UDMH and $N_2O_4$ do not exist in the gaseous phase but decompose into other products. Within the context of this paper, this denomination is relative to the decomposition products. The liquid phase is composed

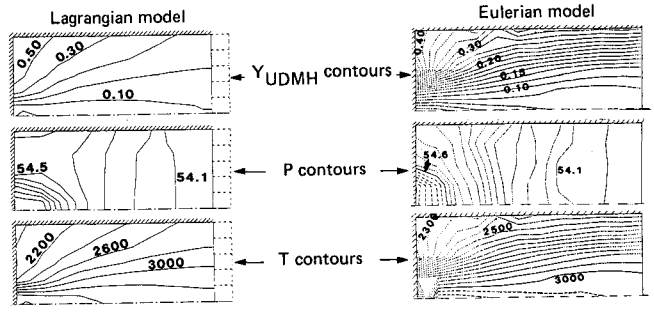


**Fig. 2 Gaseous UDMH mass fraction ($Y_{UDMH}$), pressure and temperature contours: comparison between results issued from Lagrangian and Eulerian models.**

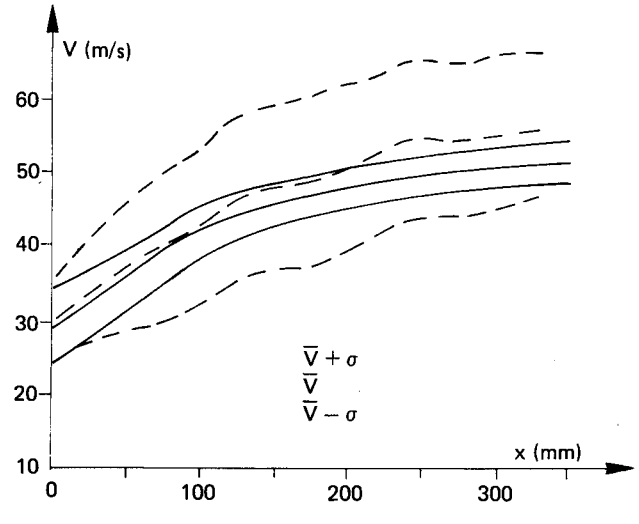


**Fig. 1 Droplet velocity profiles along the chamber axis: comparison between numerical and experimental data ($\bar{V}$ mean value; $\sigma$, standard deviation)—numerical,---experimental.**

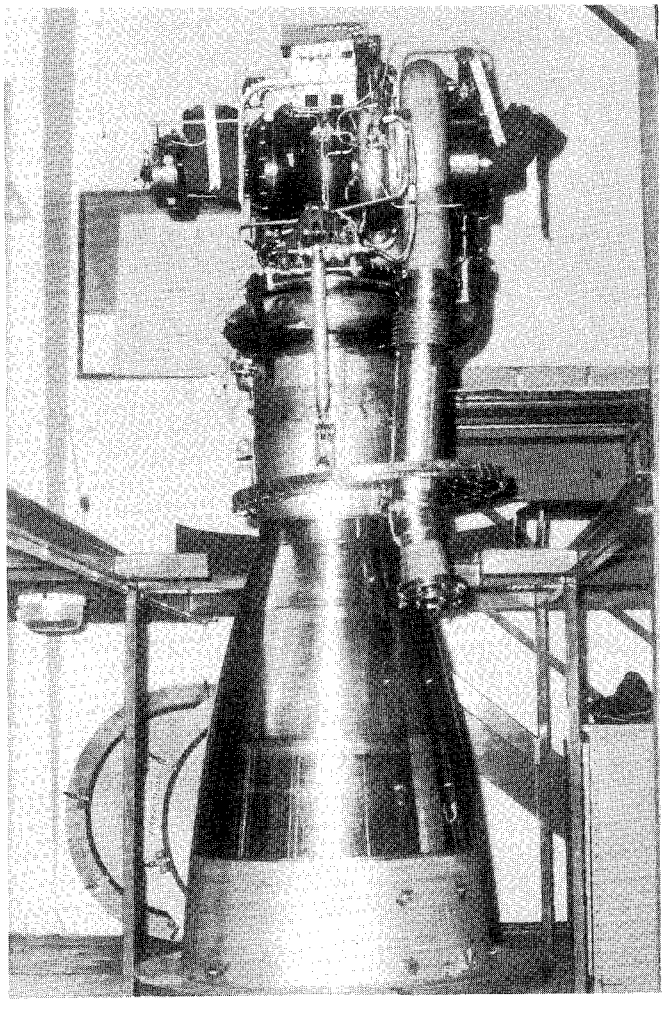

**Fig. 3 Viking engine—(Société Européenne de Propulsion photography).**

of groups; each group includes droplets of the same chemical components having the same mean diameter, velocity, and temperature at injection.

For the gaseous phase, the Navier-Stokes equations with source terms are solved and for the liquid phase, a set of balance equations for each group is solved by means of an Eulerian method.

*Gaseous Phase*

Continuity equation for the total mass

$$\frac{\partial \rho}{\partial t}+\frac{\partial \rho u}{\partial z}+\frac{\partial \rho v}{\partial y}=\dot{w}-\rho u\frac{1}{b}\frac{db}{dz} \tag{1}$$

Fuel ($k=1$) and oxidizer ($k=2$) transport equations

$$\frac{\partial \rho_k}{\partial t}+\frac{\partial \rho_k u}{\partial z}+\frac{\partial \rho_k v}{\partial y}=\dot{w}_k+\frac{\partial}{\partial z}\left[\rho D\frac{\partial}{\partial z}\left(\frac{\rho_k}{\rho}\right)\right]+\frac{\partial}{\partial y}\left[\rho D\frac{\partial}{\partial y}\left(\frac{\rho_k}{\rho}\right)\right]-\left[\rho_k u-\rho D\frac{\partial}{\partial z}\left(\frac{\rho_k}{\rho}\right)\right]\frac{1}{b}\frac{db}{dz} \tag{2}$$

The burned products ($k=3$) partial density is given by

$$\rho_3=\rho-(\rho_1+\rho_2)$$

*Axial Momentum, z-axis*

$$\frac{\partial \rho u}{\partial t}+\frac{\partial \rho u^2}{\partial z}+\frac{\partial \rho uv}{\partial y}=-\frac{\partial p}{\partial z}+\frac{\partial \sigma_{zz}}{\partial z}+\frac{\partial \sigma_{zy}}{\partial y}+f_z+S_{qz}-\rho u^2\frac{1}{b}\frac{db}{dz} \tag{3}$$

*Transverse Momentum, y-axis*

$$\frac{\partial \rho u}{\partial t}+\frac{\partial \rho uv}{\partial z}+\frac{\partial \rho v^2}{\partial y}=-\frac{\partial p}{\partial y}+\frac{\partial \sigma_{zy}}{\partial z}+\frac{\partial \sigma_{yy}}{\partial y}+f_y+S_{qy}-\rho uv\frac{1}{b}\frac{db}{dz} \tag{4}$$

The $f_z$ and $f_y$ are the particle drag components in the $z$ and $y$ directions. $S_{qz}$ and $S_{qy}$ are the momentum exchanges between the two phases due to evaporation in the $z$ and $y$ directions, respectively. The $\sigma_{zz}$, $\sigma_{yy}$, and $\sigma_{zy}$ are the viscous stresses.

*Energy*

$$\frac{\partial \rho e}{\partial t}+\frac{\partial \rho eu}{\partial z}+\frac{\partial \rho ev}{\partial y}=-p\left(\frac{\partial u}{\partial z}+\frac{\partial v}{\partial y}\right)+\sigma_{zz}\frac{\partial u}{\partial z}+\sigma_{yy}\frac{\partial v}{\partial y}+\sigma_{zy}\left(\frac{\partial u}{\partial y}+\frac{\partial v}{\partial z}\right)-\frac{\partial q_z}{\partial z}-\frac{\partial q_y}{\partial y}+S_e-\rho eu\frac{1}{b}\frac{db}{dz}-pu\frac{1}{b}\frac{db}{dz}+(\sigma_{zz}u+\sigma_{zy}v)\frac{1}{b}\frac{db}{dz}-q_z\frac{1}{b}\frac{db}{dz} \tag{5}$$

$S_e$ is the energy exchange term, to be given later; $q_z$ and $q_y$ are the heat fluxes due to both conduction and diffusion:

$$q_z=-\lambda\frac{\partial T}{\partial z}-\rho D\sum_k h_k\frac{\partial}{\partial z}\left(\frac{\rho_k}{\rho}\right)$$

$$q_y=-\lambda\frac{\partial T}{\partial y}-\rho D\sum_k h_k\frac{\partial}{\partial y}\left(\frac{\rho_k}{\rho}\right)$$

The $\lambda$ is thermal conductivity, $h_k$ is the specific enthalpy of species $k$, and $D$ is the species diffusivity.

Temperature is then obtained from the specific internal energy using the relation

$$e(T)=\sum_k\frac{\rho_k}{\rho}e_k(T)$$

Pressure is given by the perfect gas law

$$p=RT\sum_k\frac{\rho_k}{M_k}$$

*Liquid Phase*

For each group $m$, the following equations are solved.

Continuity equation

$$\frac{\partial \rho_m}{\partial t}+\frac{\partial \rho_m u_m}{\partial z}+\frac{\partial \rho_m v_m}{\partial y}=\dot{w}_m-\rho_m u_m\frac{1}{b}\frac{db}{dz}+(\dot{\rho}_m)_{ri} \tag{6}$$

The $\dot{w}_m$ is the rate of change of $\rho_m$ caused by vaporization. The $(\dot{\rho}_m)ri$ is the rate of change $\rho_m$ due to radial injection.

For a given injection cell, this term is given by

$$(\dot{\rho}_m)_{ri}=\frac{\dot{m}_{\text{inj}}}{V_{\text{cell}}} \tag{7}$$

$V_{\text{cell}}$ is the cell volume; and $\dot{m}_{\text{inj}}$ is the mass flow rate injected in this cell.

*Axial Momentum, z-axis*

$$\frac{\partial \rho_m u_m}{\partial t}+\frac{\partial \rho_m u_m^2}{\partial z}+\frac{\partial \rho_m u_m v_m}{\partial y}=f_{mz}+S_{qmz}-\rho_m u_m^2\frac{1}{b}\frac{db}{dz}+\overline{(\dot{\rho}_m u_m)}_{ri} \tag{8}$$

The $\overline{(\dot{\rho}_m u_m)}_{ri}$ is the axial momentum source term due to radial injection.

It is given by

$$\overline{(\dot{\rho}_m u_m)}_{ri}=\frac{\dot{m}_{\text{inj}}u_i}{V_{\text{cell}}}$$

where $u_i$ is the axial component (if any) of the injection velocity. The $f_{mz}$ is the drag component in the $z$ direction; $S_{qmz}$ is the momentum exchange between the gaseous phase and group $m$ in the $z$ direction.

*Transverse Momentum, y-axis*

$$\frac{\partial \rho_m v_m}{\partial t}+\frac{\partial \rho_m u_m v_m}{\partial z}+\frac{\partial \rho_m v_m^2}{\partial y}=f_{my}+S_{qmy}-\rho_m u_m v_m\frac{1}{b}\frac{db}{dz} \tag{9}$$

The $f_{my}$ is the drag component in the $y$ direction; $S_{qmy}$ is the momentum exchange between the gaseous phase and group $m$ in the $y$ direction.

*Droplet Number Balance Equation*

$$\frac{\partial n_m}{\partial t}+\frac{\partial n_m u_m}{\partial z}+\frac{\partial n_m v_m}{\partial y}=-n_m u_m\frac{1}{b}\frac{db}{dz}+(\dot{n}_m)_{ri}$$

The $(\dot{n}_m)_{ri}$ is the rate of change of $n_m$ resulting from radial injection

$$(\dot{n}_m)_{ri}=\frac{(\dot{\rho}_m)_{ri}}{\frac{\pi}{6}D_i^3\rho_L}$$

where $D_i$ is the diameter of the droplets radially injected, and $\rho_L$ is the density of the liquid jet.

For the energy equation, we neglect the heating period by assuming that the droplet surface reaches the vaporization temperature very rapidly and remains constant. This assumption is valid when thermal transfers inside the droplet are slow as is the case with no convection. This model will have to be improved if it is to take into account the convection effect on thermal transfers into the droplet.

### B. Input Data

Running this numerical code for spray combustion simulation requires atomization and droplet-combustion data. These two topics are discussed below.

*Atomization Study*

The atomization study[2] consisted of the experimental characterization of the spray issued from like-on-like doublet for the DEV injector (development injector) and the TA5S injector (postfailure injector).

Test results showed that the size distribution issued from a like-on-like doublet may be represented by a Rosin-Rammler law

$$g(D) = \frac{N}{\bar{D}}\left(\frac{D}{\bar{D}}\right)^{N} e^{-(D/\bar{D})^{N}}$$

where $N$ and $\bar{D}$ are fitting parameters.

In such a case, the mass median diameter $D_M$ and the Sauter mean diameter $D_{32}$ are given by

$$D_M = \bar{D}(\ell n 2)^{1/N}$$

$$D_{32} = \frac{\bar{D}}{\Gamma[1-(1/N)]}$$

where $\Gamma$ is the gamma function.

For the Viking engine, the following expressions have been obtained to represent $D_M$ and $N$:

UDMH-type doublet

$$D_M(\mu\text{m}) = 76\left(\frac{V_j \text{m/s}}{30}\right)^{-0.95}\left(\frac{D_j \text{mm}}{2.9}\right)^{0.3}\left(\frac{L_j \text{mm}}{4.9}\right)^{-0.08} \times \left(\frac{\rho \text{kg/m}^3}{5}\right)^{-0.2}$$

$$\frac{1}{N} = \frac{1}{2.75} - 0.19 \log_{10}\left(\frac{\rho \text{ kg/m}^3}{5}\right)$$

$N_2O_4$-type doublet

$$D_M(\mu\text{m}) = 138\left(\frac{V_j \text{m/s}}{30}\right)^{-0.95}\left(\frac{D_j \text{mm}}{4.3}\right)^{0.3}\left(\frac{L_j \text{mm}}{4.9}\right)^{-0.08} \times \left(\frac{\rho \text{ kg/m}^3}{5}\right)^{-0.2}$$

$$\frac{1}{N} = \frac{1}{2.35} - 0.13 \log_{10}\left(\frac{\rho \text{ kg/m}^3}{5}\right)$$

$D_j$ = the injection hole diameter
$L_j$ = the liquid-jet length
$V_j$ = the absolute liquid-jet velocity
$\rho$ = the ambient gas density

The geometrical data of the two injectors (DEV and TA5S) are given in Table 1.

*Droplet-Combustion Study*[3]

The method consisted of two numerical codes: an easy to use, one-dimensional model taking into account the physicochemical phenomena involved in the droplet combustion process and a second two-dimensional one, which includes convective effects on the vaporization. The numerical approach consists of solving the balance equations for the incompressible phase (droplet) and for the surrounding gas. For the gas, the Navier-Stokes equations are solved. Inside the droplet, the temperature is obtained from the energy equation, and the velocity is given by the Hill vortex approach.

**Table 1 Injector geometrical data**

| Injector | Parameter $L_j$, mm | Parameter $D_j$, mm: UDMH doublet | Parameter $D_j$, mm: $N_2O_4$ doublet |
|---|---|---|---|
| DEV | 4.9 | 2.7 | 3.9 |
| TA5S | 4.9 | 2.9 | 4.3 |

For systematic use, an analytical vaporization law was derived from numerical computations as shown below.

Analytical expressions of the vaporization-combustion laws of UDMH and $N_2O_4$ droplets have been found to fit numerical calculations performed by means of the droplet-combustion code.

UDMH vaporization law

$$\dot{m}_0 = (955 + 2.10^{-5}\, p)10^{-6}\, D^{1.1}\left(\frac{D}{D_0}\right)^{0.4} \times \ell n(1+B)\left[1 + 1100 D^{3.5}\left|\frac{dp}{dt}\right|\right] - 1.06\ 10^{-8}\, D_0 D^{1.5}\frac{dp}{dt}$$

with $B = 0.002\ (T_\infty - T_{CU}) + 14\ Y_{N\infty}$.

$N_2O_4$ vaporization law

$$\dot{m}_0 = \left[1278 + (426 + 1.7\ 10^{-5}\, p)\left(\frac{D}{D_0}\right)^2\right] 10^{-6} D\, \ell n(1+B) - 1.2\ 10^{-6}\, D^3 \frac{dp}{dt}$$

with $B = 0.00028\ (T_\infty - T_{CN}) + 3\ Y_{U\infty}$.

$D_0$ is the diameter at injection; $T_\infty$ is the ambient temperature; $T_{CU}$ and $T_{CN}$ the critical temperatures of UDMH and $N_2O_4$, respectively, and $Y_{U\infty}$ and $Y_{N\infty}$ the ambient mass fractions of gaseous UDMH and gaseous $N_2O_4$, respectively.

The preceding expressions were established without convection. Computations taking into account a droplet-gas relative velocity have been performed, and it has been found that the convection effects are well correlated by the classical Ranz-Marshall correction[4]

$$\dot{m} = \dot{m}_0(1 + 0.3\, Re^{1/2} Pr^{1/3})$$

where $\dot{m}_0$ is the vaporized mass flow rate without convection; $Re$ the Reynolds number based on the relative velocity; and $Pr$ the Prandtl number.

### C. Droplet-Gas Interaction

Droplets interact with the gaseous phase through mass exchange, momentum exchange, and energy exchange. The expressions of the exchange terms are given below.

The mass loss as a result of vaporization [Eq. (6)] is given by

$$\dot{w}_m = -n_m \dot{m}$$

The rate of change of the total density [Eq. (1)] is

$$\dot{w} = -\sum_m \dot{w}_m$$

The rate of change of the partial densities of UDMH and $N_2O_4$ consists of two terms

$$\dot{w}_k = \dot{w}_k^c + \dot{w}_k^v$$

The $\dot{w}_k^c$ is the mass loss as a result of the chemical reactions, and $\dot{w}_k^v$ is the mass production as a result of the vaporization of the droplets of the same chemical components as the species $k$

$$\dot{w}_1^v = -\sum_{\substack{\text{UDMH}\\ \text{groups}}} \dot{w}_m \quad \text{and} \quad \dot{w}_2^v = -\sum_{\substack{\text{N}_2\text{O}_4\\ \text{groups}}} \dot{w}_m$$

A one-step chemical reaction has been assumed

$$\text{UDMH} + a\text{N}_2\text{O}_4 \rightarrow \text{Products}$$

with a rate

$$\dot{\omega} = CC(\rho_1/M_1)(\rho_2/M_2)^a, \qquad CC = 10^5, \qquad a = 1.203$$

$$\dot{w}_1^c = -M_1\dot{\omega}, \qquad \dot{w}_2^c = -aM_2\dot{\omega}$$

Two turbulent combustion models were used in the two-dimensional $(x,y)$ Lagrangian model to simulate the flow in the two-dimensional transparent chamber. These models are the Magnussen model[5] and the one mentioned above. The latter is an asymptotical case of the Arrhenius model as the ratio $T_A/T$ approaches zero; $T_A$ is the activation temperature and $T$ the gas temperature. Results showed that the Magnussen model leads to a lower combustion temperature and thus to a combustion efficiency lower than the transparent chamber one. The above combustion model gave the most realistic results. Moreover, visual observation of the reacting flow in the two-dimensional transparent, combustion chamber confirmed that the reaction zone locations were better predicted when using the above combustion model than when using the Magnussen model.

The particle drag components [Eqs. (7) and (8)] are give by

$$f_{mz} = \frac{\pi}{8}\mu_g n_m D_m C_{xm} Re_m (u - u_m)$$

$$f_{my} = \frac{\pi}{8}\mu_g n_m D_m C_{xm} Re_m (v - v_m)$$

$$Re_m = \frac{\rho D_m}{\mu_g}\left[(u-u_m)^2 + (v-v_m)^2\right]^{1/2}$$

where $Re_m$ is the Reynolds number, and $C_{xm}$ is the drag coefficient.

The droplet-combustion study[3] also showed that the evaporating droplet drag coefficient is approximately one-half the drag coefficient of a non-evaporating droplet because the role played by the friction forces is significantly reduced for a vaporizing droplet as a result of the boundary-layer blowing. On the other hand, the role of the pressure forces is not greatly modified by vaporization.

The following relations were used for the drag coefficient:

$$C_{xm} = (12/Re_m)(1 + 0.15\, Re_m^{0.687}) \qquad \text{if } Re_m \le 1000$$

$$C_{xm} = 0.22 \qquad \text{if } Re_m > 1000$$

Assuming the vapor (fuel or oxidizer) has the same velocity as the droplet when it leaves the surface, the momentum loss may be written as

$$S_{qmz} = \dot{w}_m u_m \qquad S_{qmy} = \dot{w}_m v_m$$

Momentum source terms which appear in the gaseous phase equations [Eqs. (3) and (4)] may be written as

$$f_z = -\sum_m f_{mz} \qquad f_y = -\sum_m f_{my}$$

$$S_{qz} = -\sum_m S_{qmz} \qquad S_{qy} = -\sum_m S_{qmy}$$

From the previous assumptions, the specific internal energy source terms $S_e$ [see Eq. (5)] can be written

$$S_e = \left(h_U - \frac{R}{M_1}T_{VU}\right)\dot{w}_1^v + \left(h_N - \frac{R}{M_2}T_{VN}\right)\dot{w}_2^v - \sum_m \frac{1}{2}\dot{w}_m[(u-u_m)^2 + (v-v_m)^2]$$

The $h_U$ and $h_N$ are the specific enthalpies of liquid UDMH and liquid $N_2O_4$ at the injection temperature, respectively. $T_{VU}$ and $T_{VN}$ are the vaporization temperatures of UDMH and $N_2O_4$, respectively.

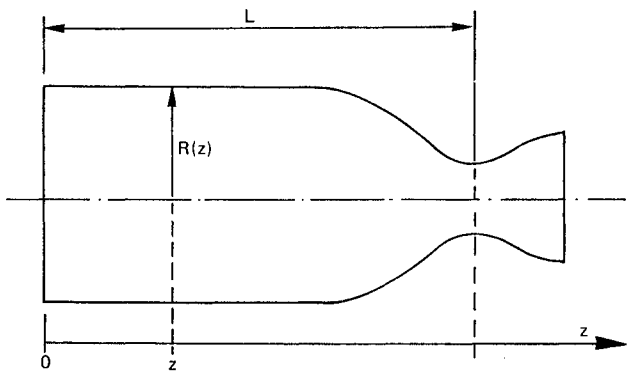


a)

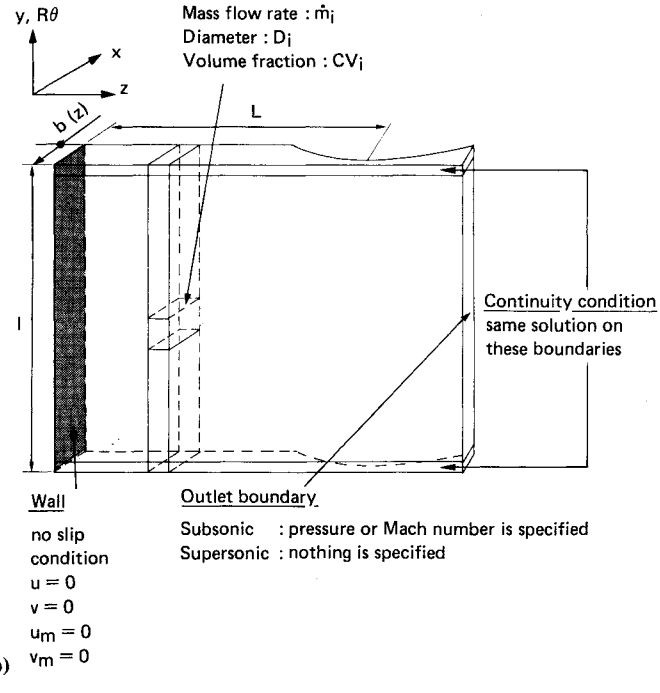


b)

**Fig. 4 Fitted geometry and boundary conditions: a) actual geometry, b) computational annular geometry.**

### D. Turbulence Model and Transport Coefficients

Effects of turbulence are taken into account by means of the subgrid scale (SGS) turbulence model.[6] Turbulent viscosity is given by

$$\mu_t = C_t \rho \, \Delta^2 \left[ 2\left(\frac{\partial u}{\partial z}\right)^2 + 2\left(\frac{\partial v}{\partial y}\right)^2 + \left(\frac{\partial u}{\partial y} + \frac{\partial v}{\partial z}\right)^2 \right]^{1/2}$$

$C_t$ is a constant of the magnitude of 0.04, and $\Delta$ is the minimum cell size.

Turbulent contributions to the transport coefficients (viscosity, thermal conductivity, and species diffusivity) are added to the laminar ones.

Turbulent thermal conductivity and species diffusivity are defined as

$$\lambda_t = \frac{\mu_t C_p}{Pr_t} \qquad D_t = \frac{\mu_t}{\rho Sc_t}$$

where $Pr_t$ is the turbulent Prandtl number, and $Sc_t$ is the turbulent Schmidt number.

### E. Numerical Method

The partial differential equations of droplet and gas are solved by the MacCormack scheme[7] combined with a staggered grid; fluxes are defined at the cell side, and scalar quantities are defined at the cell center. More details on the differencing technique are given in a previous paper.[8]

### F. Boundary Conditions

Boundary conditions are summarized in Fig. 4.

1) At the injection boundary, we specify for each group of droplets the volume fraction, the mass flow rate, and the diameter.

2) A no-slip boundary condition is used in the presence of a wall.

3) At the outlet boundary, a static pressure or a Mach number is specified when the flow is subsonic; no condition is required for a supersonic outlet boundary.

4) Finally, a continuity condition is applied on the upper and lower boundaries to ensure solution periodicity.

### G. Geometry Fit

Carrying out computations requires fitting the computational geometry to the actual one. As shown in Fig. 4, the axial length $L$ is the same as the length of the actual chamber. The transverse length $\ell$ is chosen so that the first tangential mode of the annular chamber is the same as for the actual chamber. Thus

$$\ell = a/f$$

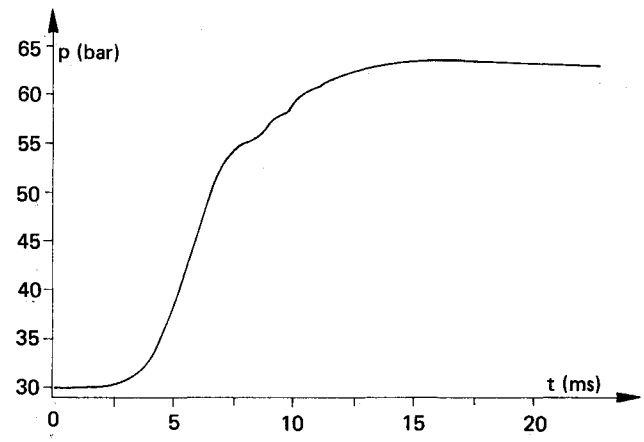


**Fig. 5 Chamber head mean pressure vs time from start up to the steady state.**

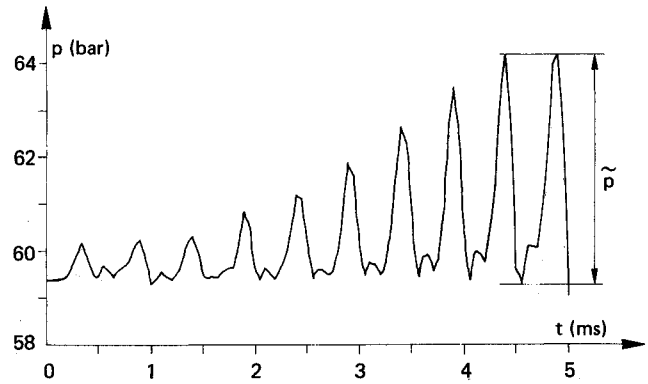


**Fig. 6 Example of instabilities for the DEV injector, nominal working point: $\dot{m} = 235$ kg/s, m = 1.86.**

where $a$ is the sound velocity and $f$ is the first tangential mode frequency of the actual chamber. The width $b(z)$ is chosen so that the cross section is the same in both geometries.

Thus, where $R(z)$ is the actual chamber radius

$$b(z) = \pi R^2(z)/\ell$$

## V. Results

High-frequency stability tests performed by the manufacturer (Société Européenne de Propulsion) on the actual engine showed the following results.[1]

1) The engine is more stable when using the TA5S injector than when using the DEV injector.

2) The stability margin decreases as the steady-state mean pressure increases.

3) The engine is more stable when the UH25 propellant (75% of UDMH + 25% of hydrazine hydrate) is used.

For numerical simulation of tangential instabilities, the

**Table 2 Computed working points**

| | Working point | | | | | | |
|---|---|---|---|---|---|---|---|
| Data | $P_1$ | $P_2$ | $P_3$ | $P_4$ | $P_5$ | $P_6$ | $P_7$ |
| Total mass flow rate $\dot{m}$, kg/s | 166.4 | 187.0 | 207.9 | 228.7 | 235.0 | 249.6 | 270.4 |
| Mixture ratio $m$ | 1.860 | 1.860 | 1.860 | 1.860 | 1.860 | 1.860 | 1.860 |

method consisted of first obtaining the steady-state solution and then applying a pressure step along the $z$ axis by setting

$$p(z,t) = \bar{p}(z)(1 + a_p), \qquad 0 \le t \le \tau_s$$

where $\bar{p}(z)$ is the steady-state pressure, $\tau_s$ is a time lag, and $a_p$ is a constant coefficient.

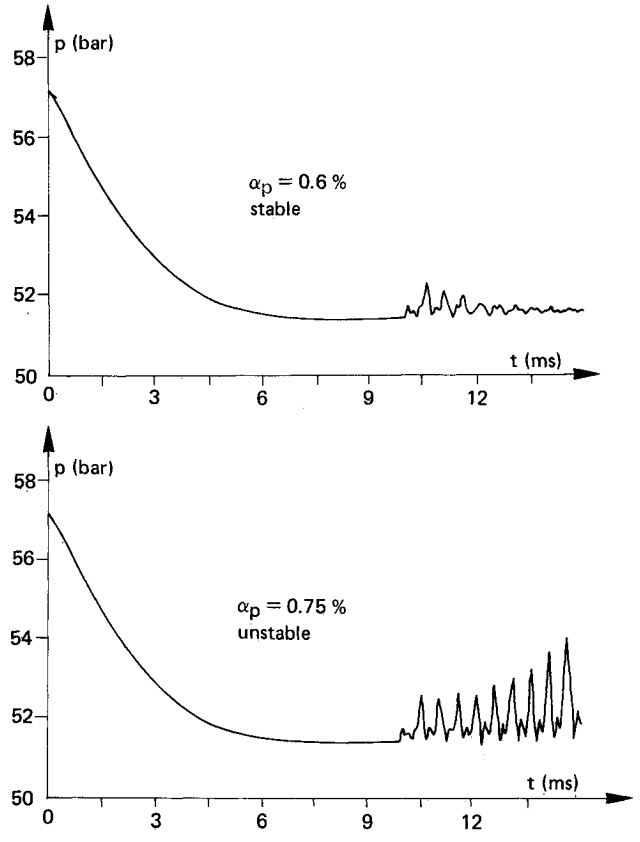


**Fig. 7 Examples of the TA5S injector response ($a_{plim}$ between 0.6% and 0.75%).**

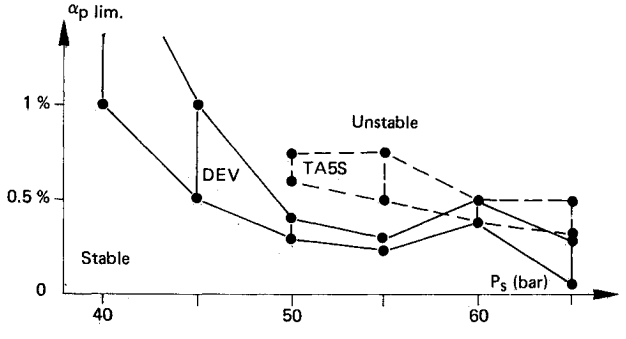


**Fig. 8a Viking engine stability results for the two injectors (DEV and TA5S); neutral stability limits vs chamber mean pressure.**

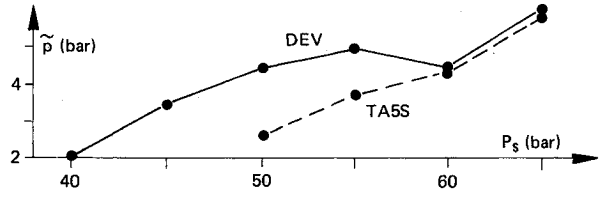


**Fig. 8b Viking engine stability results for the two injectors (DEV and TA5S); pressure level $\tilde{P}$ vs chamber mean pressure.**

The working points in Table 2 have been computed.

Figure 5 shows the chamber head mean pressure vs time from the start up to the steady-state solution. An example of instabilities after applying a pressure step is given in Fig. 6. These calculations concern the DEV injector at the nominal working point $P_5$ ($\dot{m} = 235$ kg/s and $m = 1.860$). Peak-to-peak pressure levels increase and then become constant when instabilities are well established; this constant level called $\tilde{P}$ in the figure depends on the steady-state mean pressure.

Figure 7 gives an example of excitations leading either to stable or unstable responses. These calculations concern the TA5S injector at the working point $P_3$. In this figure, the $P_3$ steady-state regime was obtained from the $P_4$ one by decreasing the mass flow rate.

After the steady-state regime is reached, an overpressure is applied. For $a_p = 0.6\%$, oscillations are damped but for $a_p = 0.75\%$, they are not. So one critical value ($a_{plim}$) corresponding to neutral stability may be defined.

Figures 8a and 8b present the final results in the form of the neutral stability curves and pressure level $\tilde{P}$ as functions of the steady-state mean pressure.

The numerical simulation fits the main features of the actual engine behavior by finding the destabilizing effect of a mean pressure increase and the stabilizing effect of the injector change (DEV → TA5S) following the failure.

The stabilizing effect of using the UH25 has yet to be studied, as data for this propellant are not well known.

## VI. Conclusion

In response to the Viking engine instability problem, a study including both numerical and experimental aspects was undertaken. On the experimental side, the atomization study provided the characterization of the spray issued from the Viking engine injector. On the numerical side, one distinguishes the droplet-combustion model and the chamber model. The droplet-combustion model led to the droplet vaporization laws. For the chamber, two numerical models were developed: a planar two-dimensional Lagrangian model and an Eulerian annular model called PHEDRE. The Lagrangian model can be used to describe the steady-state regime in detail. The annular model is suitable for unsteady numerical simulation. They both employ the atomizaton and the droplet-combustion results.

The PHEDRE code was used to simulate tangential instabilities. The latter were triggered by a pressure step. Results showed that for each working point, a critical value ($a_{plim}$) of the pressure step exists. When the overpressure exceeds this critical value, pressure oscillations are not damped.

The following results were obtained.

1) The critical value of the overpressure decreases—and thus engine stability—when the chamber pressure increases.

2) The TA5S injector (postfailure injector) is more stable than the DEV injector (development injector).

3) When instability occurs, peak-to-peak pressure levels increase when the chamber pressure increases.

All these features were observed on the actual engine during test runs.

The approach used for the Viking engine is being applied to stability studies for both the future Ariane 5 HM60 cryogenic engine (using hydrogen and oxygen) and for the L5 stage 20 kN engine [using hypergolic propellant: monomethyl hydrozine (MMH) and $N_2O_4$].

## References

[1]Souchier, A., Lemoine, J. C., Dorville, G., "Résolution du Problème des Instabilités sur le Moteur Viking," *Proceedings of the 33rd International Astronautical Federation Congress*, IAF Paper 82-363, AIAA, New York, 1982.

[2]Lourme, D., "Like-on-Like Injector Spray Characterization for the Ariane Viking Engine," AIAA Paper 86-1444, June 1986.

[3]Scherrer, D., "Effet de la Convection sur l'Évaporation et la Combustion d'une Goutte de Combustible," *70th AGARD PEP: Symposium on Combustion and Fuel in Gas Turbine Engines,* AGARD, CP 422, Oct. 1987, pp. 39-1-39-8.

[4]Ranz, W. E., Marshall, W. R., "Evaporation from Drops—Part I," Chemical Engineering Progress, Vol. 48, 1952, No. 3, pp. 141–146.

[5]Magnussen, B. F., "On the Structure of Turbulence and a Generalized Eddy Dissipation Concept for Chemical Reaction in Turbulent Flow," AIAA Paper 81-0042, Jan. 1981.

[6]Deardoff, J. W., "On the Magnitude of the Subgrid Scale Eddy Coefficient," *Journal of Computational Physics,* Vol. 7, 1971, pp. 120–133.

[7]MacCormack, R. W., "The Effect of Viscosity in Hypervelocity Impact Cratering," AIAA Paper 69–354, 1969.

[8]Habiballah, M., and Monin, H., "Two-Dimensional Model for the Two-Phase Flow Simulation in a Viking Rocket Engine Combustion Chamber," *Proceedings of the 9th International Conference on Numerical Methods in Fluid Dynamics,* Springer-Verlag, Berlin, 1984, pp. 255–261.